Sign change of the extrinsic spin Hall effect in binary alloys

Lei Wang [*]

*Key Laboratory of Quantum Materials and Devices of Ministry of Education, School of Physics, Southeast University, Nanjing 211189, China
and Center for Spintronics and Quantum Systems, State Key Laboratory for Mechanical Behavior of Materials,
Xi'an Jiaotong University, No. 28 Xianning West Road Xi'an, Shaanxi 710049, China*

The spin Hall effect and its inverse have supported charge-spin conversion in spintronics for a long time, and a large spin Hall angle, which corresponds to the charge-spin conversion efficiency, is always needed for fast magnetic switching and energy conservation. Conventionally, the spin Hall angles in alloys are larger than those in pure metals with similar structures and elements, making them competitive candidates in spintronics. However, along with the introduction of disorder, the extrinsic spin Hall effect dominates and remains unclear because the corresponding sign could be different between experiments and theoretical calculations. Here, the first-principles-based scattering wave approach is used for binary Pt_xPd_{1-x} and Au_xAg_{1-x} alloys. The spin Hall effect therein is systematically studied, and the results reveal that the sign of the anomalous Hall angle can be changed by the components of the alloys in the dilute region due to the competition between different contributions. Our findings contribute to the understanding of the spin Hall effect in alloys and indicate that the localized clusters in dilute alloys should be the key to the sign difference in the spin Hall effect between theoretical and experimental results.

I. INTRODUCTION

The spin Hall effect, as an efficient charge-spin conversion mechanism, plays an important role in the field of spintronics [1,2] and can generate spin-orbit torque (SOT) in bilayer systems to switch the magnetization [3–5] and be applied to magnetic random access memory (MRAM) to reduce the writing current for low-energy consumption and high operation speed [6–8]. As the spin Hall angle gives the charge-spin conversion efficiency, a large spin Hall angle is always imperative for applications. Therefore, many materials have been studied and been reported to have large spin Hall angles, such as metallic Pt [9–11], β-W [12–15], β-Ta [3,16–19], and topological insulators [20–24]. However, the intrinsic strong spin-orbit coupling therein leads to high resistivity and a short spin diffusion length, which limit their application prospects in chips. Based on these considerations, dilute alloys with light element seeds and slight heavy element doping become competitive candidates that can combine the advantages of low resistivity, long spin diffusion length, and a large spin Hall angle.

The whole story and mystery of the spin Hall effect in dilute alloys began with the measurement of the spin Hall angle of Au in an FePt/Au bilayer using a nonlocal technique [25]. The reported spin Hall angle therein is approximately 0.113, which is significantly large and beyond the commonsense value for the weak spin Hall effect in bulk Au. Therefore, Guo *et al.* [26] proposed the possibility of an extra contribution from the Fe impurity and the corresponding resonant skew

scattering to explain this large spin Hall effect. However, Gradhand *et al.* [27,28] carried out spin Hall angle calculations by introducing multiple impurities and demonstrated that the slight C or N impurities introduced in the thin-film growth process should be the key. Although clarifying the origin of the giant spin Hall angle of Au in experiments is challenging, the information that minor impurities may enormously enhance the spin Hall angle has inspired many studies on dilute alloys [29–34], such as CuBi and CuIr. Furthermore, there appears to be another difficult problem as shown in Table I: For example, the sign of the spin Hall angle obtained by theoretical calculations [28,35] is different from that measured by experiments for CuBi [29], which may be attributed to a phase shift [35,36] or electron correlations [37,38].

To clarify this sign problem in dilute alloys, in this paper, first-principles calculations based on the scattering wave-function method are carried out. Typically, to avoid mismatch of the crystal structure, Pt_xPd_{1-x} and Au_xAg_{1-x} alloys are chosen. The calculation results reveal that the skew-scattering and side-jump contributions for $x \to 0$ and $x \to 1$ could be significantly different, which results in a concentration-dependent sign change of the spin Hall effect. Moreover, by analyzing the competition of the contributions in binary alloys, the formation of localized clusters can potentially be considered as one of the elements explaining the difference in sign between theoretical and experimental works.

II. MODEL AND METHOD

The two-lead model from Ando [45] is an efficient method to calculate the transport properties of the materials, where the calculated structure is constructed by two semi-infinite

*wanglei.icer@seu.edu.cn

TABLE I. The signs of spin Hall effect obtained in previous theoretical and experimental studies for different $X(Y)$ alloys with minor impurity Y in X. Here, "P" represents positive, "N" stands for negative, and "A" means the results are adjustable by tuning parameters.

Alloys	Theory	Experiment
Cu(Bi)	P [28]; A [35,36]	N [29]
Cu(Ir)	A [38]	P [29]; P [39]
Cu(Pt)	P [28]	P [40]; P [41]
Au(Pt)	P [42]; P [28]	P [43]
Pt(Au)	P [42]; N [28]	P [43]
Au(Cu)	N [28]	P [44]
Pt(Cu)	N [28]	P [41]

crystallines ($\mathcal{L}$-Lead and $\mathcal{R}$-Lead) and one scattering region as shown in the inset of Fig. 1, respectively. Technically, the corresponding formalism was realized based on a tight-binding (TB) muffin-tin orbital (MTO) [46] within the local-spin-density approximation (LSDA) of density-functional theory (DFT) and then promoted to a spin-orbit coupling version using a perturbation approach [47]. This method is compatible with many kinds of disorders, such as impurity [46,48–50], phonon [51–57], and magnon [56,57], which have been demonstrated to be able to recover the temperature dependences of the resistivity, spin diffusion length, and spin Hall effect observed in experiments [55–60].

Furthermore, as the conventional MTO basis was updated to the exact muffin-tin orbitals (EMTOs) [61,62] and a fully relativistic (FR) effect [63,64] can be introduced to describe the Hamiltonian with spin-orbit coupling more precisely, we combined them with the previous TB-MTO codes to realize the FR-EMTO transport code [65–67], accordingly.
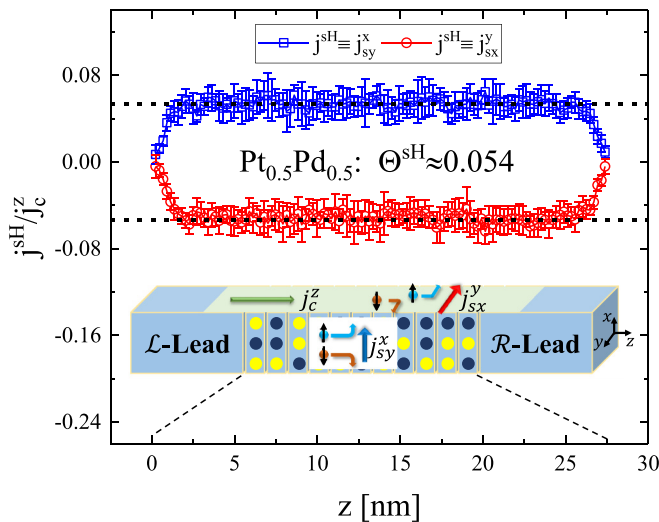

FIG. 1. Normalized spin Hall current j^{sH} as a function of z inside the scattering region and estimated effective spin Hall angle Θ^{sH}. The inset shows the calculation model with two ideal leads sandwiching a scattering region, the arrows illustrate the corresponding charge and spin currents in the system, and the dashed lines display the range of z coordinates of the scattering region.

A. Spin Hall effect

As described in Ref. [65], the charge current operator generated from atom R' to atom R reads as

$$J_{RR'} = \frac{1}{i\hbar}[\langle \Psi_R | \hat{\mathcal{H}}_{RR'} | \Psi_{R'} \rangle - \langle \Psi_{R'} | \hat{\mathcal{H}}_{R'R} | \Psi_R \rangle], \quad (1)$$

where $|\Psi_R\rangle$ is the scattering wave function [45–47,65] at site R and $\hat{\mathcal{H}}_{RR'}$ is the corresponding hopping Hamiltonian between atom R and atom R'. By inserting the Pauli matrix $\hat{\sigma}_{m,m\in\{x,y,z\}}$, this equation can also be used to calculate the spin current as [59,60,68]

$$J^s_{m,RR'} = \frac{1}{i\hbar}[\langle \Psi_R | \mathcal{T}_{RR'} | \Psi_{R'} \rangle - \langle \Psi_{R'} | \mathcal{T}_{R'R} | \Psi_R \rangle], \quad (2)$$

where $\mathcal{T}_{RR'} = \hat{\sigma}_m \hat{\mathcal{H}}_{RR'}$ and $\mathcal{T}_{R'R} = \hat{\mathcal{H}}_{R'R} \hat{\sigma}_m$. Summarizing all the above information and projecting the spin/charge current onto the global axis, as shown in the inset of Fig. 1, the spin Hall effect can be obtained. Here, one should note that j_c^z denotes the charge (c) current flowing in the z direction and j_{sy}^x represents the spin (s) current flowing in the x direction for electrons with $\hat{\sigma}_y$ polarization, for example. Thus, the spin Hall angle will be $\Theta^{sH} = j_{sy}^x/j_c^z = -j_{sx}^y/j_c^z$, with the minus sign coming from the definition of the global axis.

B. Computational details

For all calculations, the transport direction (z) is along the fcc [111] direction, and a 6×6 lateral supercell with periodic boundary conditions in the x-y plane is used to generate the alloy by randomly placing different atoms according to the corresponding concentration. To ensure that the results converge, the supercell Brillouin zone (BZ) is sampled with 32×32 k points, the disordered scattering region for the alloy is $\sim$27 nm long, and ten random disorder configurations are calculated. Typically, for $Pt_{0.5}Pd_{0.5}$, as shown in Fig. 1, the calculated spin Hall currents j_{sy}^x and j_{sx}^y are almost constant except at the interfaces between the leads and the scattering region. Therefore, the spin Hall angle of the bulk alloy can be estimated by averaging the interior results far from the interfaces, e.g., as shown by the dashed lines in Fig. 1, and the spin Hall angle of $Pt_{0.5}Pd_{0.5}$ is approximately $\Theta^{sH} \simeq 0.054$. Here, to avoid misleading results, $\Theta^{sH} = j_{sy}^x/j_c^z$ is used and will be the default option in the rest of the paper.

III. RESULTS AND ANALYSIS

By changing the concentration x, the corresponding spin Hall angles for Au_xAg_{1-x} and Pt_xPd_{1-x} alloys in the dilute region can be calculated, and the results are plotted in Figs. 2(a) and 2(d), respectively. Unsurprisingly, the absolute values of the spin Hall angles are much larger with $x > 0.99$ than with $x < 0.01$, and one may note that for the clean limit of the alloys ($x \to 0$ or $x \to 1$), the spin Hall angles remain at a significant value for the Au- and Pt-rich cases but almost vanish for the Ag- and Pd-rich cases; these phenomena occur because the spin-orbit coupling strength is stronger when the heavy elements Au and Pt constitute the main components of the alloys and the spin Hall effect is proportional to the spin-orbit coupling strength, conventionally. Moreover, the corresponding longitudinal resistivity ρ_L can also be calculated at the same time, and the results are
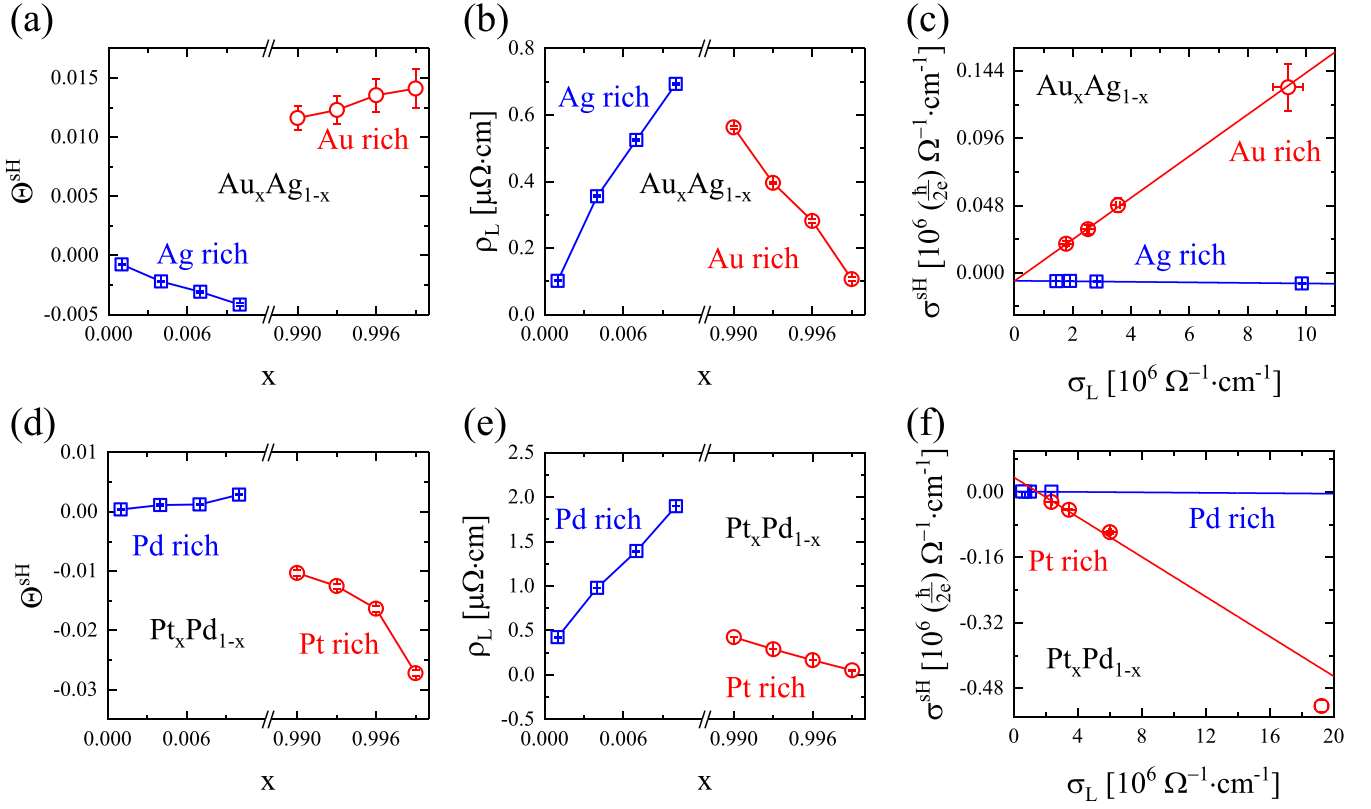
FIG. 2. Spin Hall effect-related parameters of Au_xAg_{1-x} and Pt_xPd_{1-x} alloys in the dilute region. (a) and (d) plot the spin Hall angle Θ^{sH} vs the concentration x, (b) and (e) plot the corresponding longitudinal resistivity ρ_L, and (c) and (f) show the scaling law between the spin Hall conductivity σ^{sH} and longitudinal conductivity σ_L, with $\sigma_L = 1/\rho_L$ and $\sigma^{sH} = \Theta^{sH}\sigma_L$. Here, the solid lines are the linear fitting using Eq. (4).

plotted in Figs. 2(b) and 2(e). Combining the above results, the longitudinal conductivity and spin Hall conductivity are estimated by $\sigma_L = 1/\rho_L$ and $\sigma^{sH} = (\hbar/2e)\Theta^{sH}\sigma_L$ for further analysis, as shown in Figs. 2(c) and 2(f). Here, the additional factor of $(\hbar/2e)$ is the ratio between the electron spin $(\hbar/2)$ and electron charge (e) to convert the conductivity of charge to the conductivity of spin. Thus, the spin Hall angle Θ^{sH} still remains dimensionless.

More important information from Figs. 2(a) and 2(d) is that the signs of the spin Hall angles are different with $x < 0.01$ and $x > 0.99$ for both the Au_xAg_{1-x} and Pt_xPd_{1-x} alloys, indicating that the sign of the spin Hall effect strongly depends on the concentration. Here, it should be noticed that the concentration-dependent sign change of the anomalous Hall effect had been reported previously [69,70], which can be attributed to the competition between the intrinsic, side-jump, and skew-scattering contributions. Considering that, the spin Hall effect shares similar physical origins with the anomalous Hall effect, the above sign change of the spin Hall angles may be understood by a similar physical picture.

To discriminate the different contributions to the spin Hall effect in alloys to understand the corresponding sign change, the scaling law [71] is used, in which the spin Hall resistivity can be expressed as

$$\rho^{sH} = \alpha\rho_L + \beta\rho_L^2, \quad (3)$$

where β is a constant that contains both intrinsic and side-jump contributions, and α denotes the skew-scattering

coefficient. Considering the transformation equation between the spin Hall resistivity and conductivity $(\rho^{sH} \simeq \sigma^{sH}/\sigma_L^2)$, the following scaling law in the frame of conductivity can be obtained as

$$\sigma^{sH} = \alpha\sigma_L + \beta. \quad (4)$$

According to previous results [65], the scaling law works when the concentration of the minor element in the alloy is less than 1%; thus, the calculated spin Hall conductivities in the dilute region for Au_xAg_{1-x} and Pt_xPd_{1-x} are appropriate for the scaling law in Eq. (4), as shown by the linear fitting (solid lines) in Figs. 2(c) and 2(f).

The fitting parameters of Eq. (4) for Au_xAg_{1-x} and Pt_xPd_{1-x} are given in Table II, and the signs of α and β differ from each other, indicating that the overall spin Hall effect comes from the competition between α corresponding

TABLE II. Fitting parameters of Figs. 2(c) and 2(f) obtained using Eq. (4), where α, a dimensionless parameter, denotes the skew-scattering coefficient and β contains both intrinsic and side-jump contributions with units of $10^6 (\hbar/2e)\Omega^{-1}$ cm^{-1}.

| | Au_xAg_{1-x} | | Pt_xPd_{1-x} | |
	Au rich	Ag rich	Pt rich	Pd rich
α	0.015	~ 0	-0.024	~ 0
β	-0.0058	-0.0056	0.036	0.0015

to the skew scattering and the constant β. More detailed information of the spin Hall conductivity can be provided as follows: (i) For the Au-rich case, the intrinsic contribution mainly comes from Au, which is only approximately $\sigma_{\text{int}} \simeq 800 \, (\hbar/2e)\Omega^{-1}\,\text{cm}^{-1}$ [72]; thus, the corresponding side-jump contribution of the Ag impurity in Au will be $\sigma_{\text{sj}} = \beta - \sigma_{\text{int}} \simeq -6600 \, (\hbar/2e)\Omega^{-1}\,\text{cm}^{-1}$. Then, the overall spin Hall effect is dominated by the skew-scattering contribution (α) of the Ag impurity in Au, and the spin Hall conductivity remains positive, as shown in Fig. 2(c). (ii) For the Ag-rich case, the intrinsic contribution is mainly from Ag, which is negligible due to the weak spin-orbit coupling [73]; therefore, the corresponding side-jump contribution of the Au impurity in Ag will be $\sigma_{\text{sj}} \simeq \beta \simeq -5600 \, (\hbar/2e)\Omega^{-1}\,\text{cm}^{-1}$. Considering that the skew-scattering contribution (α) of the Au impurity in Ag is almost zero, the overall spin Hall effect is now dominated by the side-jump contribution of the Au impurity in Ag, and the spin Hall conductivity remains negative. (iii) For the Pt-rich case, similarly, the intrinsic contribution of Pt is approximately $\sigma_{\text{int}} \simeq 4400 \, (\hbar/2e)\Omega^{-1}\,\text{cm}^{-1}$ [74], and the side-jump contribution of the Pd impurity in Pt is approximately $\sigma_{\text{sj}} = \beta - \sigma_{\text{int}} \simeq 31\,600 \, (\hbar/2e)\Omega^{-1}\,\text{cm}^{-1}$. In this case, the corresponding skew-scattering contribution (α) of the Pd impurity in Pt dominates, and the overall spin Hall conductivity is negative. (iv) For the Pd-rich case, the intrinsic contribution of Pd is approximately $\sigma_{\text{int}} \simeq 2800 \, (\hbar/2e)\Omega^{-1}\,\text{cm}^{-1}$ [72], and the side-jump contribution of the Pt impurity in Pd is approximately $\sigma_{\text{sj}} = \beta - \sigma_{\text{int}} \simeq -1300 \, (\hbar/2e)\Omega^{-1}\,\text{cm}^{-1}$. Because the skew-scattering contribution (α) of the Pt impurity in Pd is negligible, the competition between the intrinsic and side-jump contributions makes the overall spin Hall conductivity positive.

It should be also noticed that the skew-scattering contribution for the Ag impurity in Au is much larger than that for Au impurity in Ag, which is counterintuitive due to the spin Hall effect should be proportional to the spin-orbit coupling strength. This can be understood by the scattering process, in which the electrons travel within the mean free path and all the spin-orbit coupling of the related atoms inside the mean free path should be considered. Therefore, for the case with Ag impurity in Au, the effective spin-orbit coupling is mainly from the Au; for the case with Au impurity in Ag, the effective spin-orbit coupling is mainly from the Ag. Then the effective spin-orbit coupling is stronger for the first case, and the corresponding skew scattering is larger. Similar discussions can be applied to the results of $\text{Pt}_x\text{Pd}_{1-x}$.

The sign change of the spin Hall angle as a function of the concentration provides evidence that the corresponding sign is strongly dependent on the detailed impurity distribution of the materials. For example, for a given dilute alloy with 1% Ag and 99% Au, there could be two different types of alloys as shown in the insets of Fig. 3, where one is a conventional homogeneous alloy of $\text{Au}_{0.99}\text{Ag}_{0.01}$, and in the other case, the Ag can form very small localized clusters of $\text{Au}_{0.01}\text{Ag}_{0.99}$ that are surrounded by pure Au environment. These two types of alloys may have different signs of spin Hall angles due to the above concentration-dependent sign change of the spin Hall effect, even though they have the same total impurity concentrations.
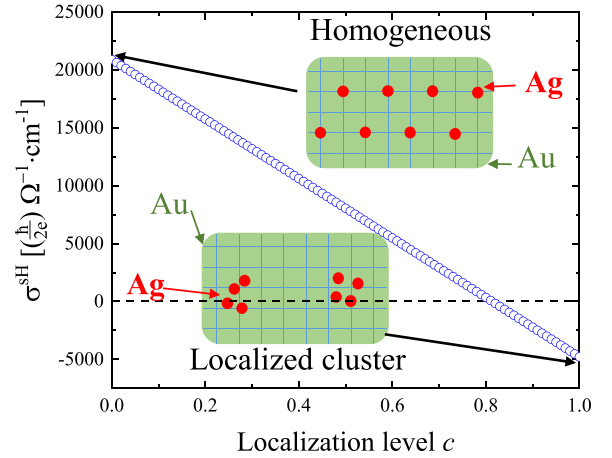

FIG. 3. Spin Hall conductivity (σ^{sH}) as a function of the localization level (c) for $\text{Au}_{0.99}\text{Ag}_{0.01}$. The insets illustrate the homogeneous alloy and localized cluster cases for understanding the sign change of the spin Hall conductivity.

On top of the above considerations, the disharmony between the theoretical calculations and experimental measurements, as illustrated at the beginning of this paper, can be reconsidered.

Let us start the discussion for the $\text{Au}_x\text{Ag}_{1-x}$ alloy with the Au-rich case. If there are some localized Ag clusters with a few Au atoms inside, then a localized Ag-rich environment appears, and all six contributions of the spin Hall effect exist. Considering the negligible intrinsic contribution of Ag and skew-scattering contribution of the Au impurity in Ag, four contributions remain, i.e., the intrinsic contribution of Au ($\sigma_{\text{int}}^{\text{Au}}$), the side-jump contribution of the Au impurity in Ag ($\sigma_{\text{sj}}^{\text{Au}}$), the side-jump contribution of the Ag impurity in Au ($\sigma_{\text{sj}}^{\text{Ag}}$), and the skew-scattering contribution of the Ag impurity in Au (α^{Ag}). We define a parameter c to describe the level of localization and assume that the total longitudinal conductivity σ_L remains constant for a given concentration x, then a simple linear combination of the spin Hall conductivity can be written as

$$\sigma^{\text{sH}} = (1 - c)\big(\alpha^{\text{Ag}}\sigma_L + \sigma_{\text{sj}}^{\text{Ag}}\big) + c\sigma_{\text{sj}}^{\text{Au}} + \sigma_{\text{int}}^{\text{Au}}. \qquad (5)$$

When $c = 0$ without any Ag clusters, Eq. (5) represents the Au-rich case, and when $c = 1$ with all Ag atoms forming clusters, only the side-jump contribution of the Au impurity in Ag and the intrinsic contribution of Au remain. Thus, Eq. (5) can be used to qualitatively analyze the localization effect.

Numerically, by putting the calculated parameters into Eq. (5), the spin Hall conductivity (σ^{sH}) as a function of the localization level (c) can be obtained, as shown in Fig. 3, which shows the sign change of the spin Hall conductivity for a given concentration $x = 0.99$.

Moreover, the previous theoretical works all focus on homogeneous alloys ($c = 0$), as shown in the inset of Fig. 3, due to the periodic boundary conditions [27,28,35]; thus, a positive spin Hall effect appears. On the contrary, the experiments have a great chance of forming small localized clusters around the surface/interface in the thin-film growth process
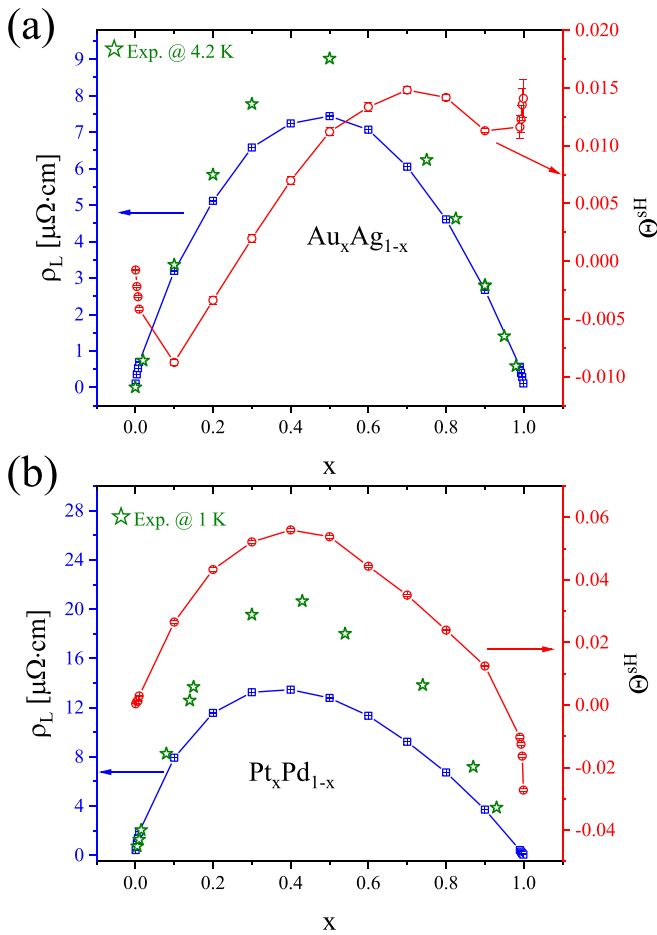
FIG. 4. Spin Hall angle (Θ^{sH}) and longitudinal resistivity (ρ_L) vs the concentration (x) of Au_xAg_{1-x} and Pt_xPd_{1-x} alloys. The green stars are the experimental measurements of the corresponding longitudinal resistivity for Au_xAg_{1-x} [75] and Pt_xPd_{1-x} [76] alloys, respectively.

according to the phase segregation [77]; therefore, if the localization effect is sufficiently strong ($c \sim 1$), then the spin Hall effect therein will be negative. Under these conditions, the disharmony between theoretical and experimental works can be attributed to the distinct microstructures of the impurity distributions (homogeneous or localized clusters) and the impurity concentration-dependent sign change of the spin Hall effect of the dilute alloys.

Furthermore, the spin Hall angles and longitudinal resistivities of Au_xAg_{1-x} and Pt_xPd_{1-x} with $x \in (0, 1)$ are calculated, and the results are plotted in Fig. 4. It can be seen that the calculated longitudinal resistivities ρ_L are close to the

experimental measurements in the dilute region ($x < 0.1$ or $x > 0.9$), but show distinct differences for the dense alloys around $x = 0.5$. The corresponding maximum differences are 17.5% for Au_xAg_{1-x} and 34.9% for Pt_xPd_{1-x}, respectively. This discrepancy may come from the polycrystalline grain boundary, defects, and other impurities in the experimental measurements, which may enhance the resistivity in experiments and are not included in the first-principles calculations. Moreover, the calculated spin Hall angles show a nonlinear curve so that the corresponding scaling law is beyond the conventional linear scaling law of Eq. (4), indicating that the competition between the contributions to the spin Hall effect from the two elements in binary alloys can be stronger in dense regions, even in homogeneous alloys.

Based on the above analysis, the spin Hall effect in binary alloys can be attributed to the competition between the six contributions, which can be split into the intrinsic contributions of the two elements if they form a quasicrystal and the side-jump and skew-scattering contributions of the scattering process between the two elements. Thus, the scaling of the spin Hall effect in binary alloys should be more complex than the conventional relation of Eq. (4), especially in dense alloys, which is why Eq. (4) can only be used when the minor element is less than 1%. Moreover, this nonlinear scaling of the spin Hall effect has already been reported based on experimental measurements of binary alloys, such as CuW [78], AuPt [43], BiSb [79], and WTa [80]. Therefore, a new scaling law for the spin Hall effect in alloys is desired and should be studied in the future.

IV. CONCLUSION

In summary, the spin Hall effect of Au_xAg_{1-x} and Pt_xPd_{1-x} alloys is systematically studied based on first-principles calculations. The skew-scattering contribution is separated out from the intrinsic and side-jump contributions in the dilute region, which show different signs. The competition between the contributions therein results in a complex scaling of the spin Hall effect and reveals that the formation of localized clusters in a dilute alloy might be at the origin of the disharmony between the theoretical and experimental studies. This work contributes to the understanding of the current experimental results of the spin Hall effect in binary alloys and will further push the study of the scaling of the spin Hall effect in binary or even more complex alloys.

[1] A. Hoffmann, IEEE Trans. Magn. **49**, 5172 (2013).

[2] J. Sinova, S. O. Valenzuela, J. Wunderlich, C. H. Back, and T. Jungwirth, Rev. Mod. Phys. **87**, 1213 (2015).

[3] L. Liu, C.-F. Pai, Y. Li, H. W. Tseng, D. C. Ralph, and R. A. Buhrman, Science **336**, 555 (2012).

[4] S. Fukami, T. Anekawa, C. Zhang, and H. Ohno, Nat. Nanotechnol. **11**, 621 (2016).

[5] W. He, C. Wan, C. Zheng, Y. Wang, X. Wang, T. Ma, Y. Wang, C. Guo, X. Luo, M. E. Stebliy, G. Yu, Y. Liu, A. V. Ognev, A. S. Samardak, and X. Han, Nano Lett. **22**, 6857 (2022).

[6] Y. C. Wu, K. Garello, W. Kim, M. Gupta, M. Perumkunnil, V. Kateel, S. Couet, R. Carpenter, S. Rao, S. Van Beek, K. K. Vudya Sethu, F. Yasin, D. Crotti, and G. S. Kar, Phys. Rev. Appl. **15**, 064015 (2021).

[7] R. Saha, Y. P. Pundir, and P. Kumar Pal, J. Magn. Magn. Mater. **551**, 169161 (2022).

[8] C. Bi, N. Sato, and S. X. Wang, in *Advances in Non-Volatile Memory and Storage Technology*, edited by B. Magyari-Köpe and Y. Nishi, Woodhead Publishing Series in Electronic and Optical Materials, 2nd ed. (Woodhead Publishing, Cambridge, U.K., 2019), pp. 203–235.

[9] L. Liu, T. Moriyama, D. C. Ralph, and R. A. Buhrman, Phys. Rev. Lett. **106**, 036601 (2011).

[10] A. Ganguly, K. Kondou, H. Sukegawa, S. Mitani, S. Kasai, Y. Niimi, Y. Otani, and A. Barman, Appl. Phys. Lett. **104**, 072405 (2014).

[11] M. Althammer, S. Meyer, H. Nakayama, M. Schreier, S. Altmannshofer, M. Weiler, H. Huebl, S. Geprägs, M. Opel, R. Gross, D. Meier, C. Klewe, T. Kuschel, J.-M. Schmalhorst, G. Reiss, L. Shen, A. Gupta, Y.-T. Chen, G. E. W. Bauer, E. Saitoh *et al.*, Phys. Rev. B **87**, 224401 (2013).

[12] C.-F. Pai, L. Liu, Y. Li, H. W. Tseng, D. C. Ralph, and R. A. Buhrman, Appl. Phys. Lett. **101**, 122404 (2012).

[13] Q. Hao and G. Xiao, Phys. Rev. Appl. **3**, 034009 (2015).

[14] R. Bansal, G. Nirala, A. Kumar, S. Chaudhary, and P. Muduli, in *2017 IEEE International Magnetics Conference (INTERMAG), Dublin, Ireland* (IEEE, New York, 2017), pp. 1–1.

[15] E. Derunova, Y. Sun, C. Felser, S. S. P. Parkin, B. Yan, and M. N. Ali, Sci. Adv. **5**, eaav8575 (2019).

[16] L. Liu, C.-F. Pai, D. C. Ralph, and R. A. Buhrman, Phys. Rev. Lett. **109**, 186602 (2012).

[17] J. E. Gómez, B. Zerai Tedlla, N. R. Álvarez, G. Alejandro, E. Goovaerts, and A. Butera, Phys. Rev. B **90**, 184401 (2014).

[18] D. Magginetti, K. Tian, and A. Tiwari, Solid State Commun. **249**, 34 (2017).

[19] R. Yu, B. F. Miao, L. Sun, Q. Liu, J. Du, P. Omelchenko, B. Heinrich, M. Wu, and H. F. Ding, Phys. Rev. Mater. **2**, 074406 (2018).

[20] N. H. D. Khang, Y. Ueda, and P. N. Hai, Nat. Mater. **17**, 808 (2018).

[21] A. R. Mellnik, J. S. Lee, A. Richardella, J. L. Grab, P. J. Mintun, M. H. Fischer, A. Vaezi, A. Manchon, E. A. Kim, N. Samarth, and D. C. Ralph, Nature (London) **511**, 449 (2014).

[22] J. Han, A. Richardella, S. A. Siddiqui, J. Finley, N. Samarth, and L. Liu, Phys. Rev. Lett. **119**, 077702 (2017).

[23] Q. Lu, P. Li, Z. Guo, G. Dong, B. Peng, X. Zha, T. Min, Z. Zhou, and M. Liu, Nat. Commun. **13**, 1650 (2022).

[24] P. Deorani, J. Son, K. Banerjee, N. Koirala, M. Brahlek, S. Oh, and H. Yang, Phys. Rev. B **90**, 094403 (2014).

[25] T. Seki, Y. Hasegawa, S. Mitani, S. Takahashi, H. Imamura, S. Maekawa, J. Nitta, and K. Takanashi, Nat. Mater. **7**, 125 (2008).

[26] G.-Y. Guo, S. Maekawa, and N. Nagaosa, Phys. Rev. Lett. **102**, 036401 (2009).

[27] M. Gradhand, D. V. Fedorov, P. Zahn, and I. Mertig, Phys. Rev. Lett. **104**, 186403 (2010).

[28] M. Gradhand, D. V. Fedorov, P. Zahn, and I. Mertig, Phys. Rev. B **81**, 245109 (2010).

[29] Y. Niimi, Y. Kawanishi, D. H. Wei, C. Deranlot, H. X. Yang, M. Chshiev, T. Valet, A. Fert, and Y. Otani, Phys. Rev. Lett. **109**, 156602 (2012).

[30] S. Ruiz-Gómez, R. Guerrero, M. W. Khaliq, C. Fernández-González, J. Prat, A. Valera, S. Finizio, P. Perna, J. Camarero, L. Pérez, L. Aballe, and M. Foerster, Phys. Rev. X **12**, 031032 (2022).

[31] P. Wang, A. Migliorini, S.-H. Yang, J.-C. Jeon, I. Kostanovskiy, H. Meyerheim, H. Han, H. Deniz, and S. S. P. Parkin, Adv. Mater. **34**, 2109406 (2022).

[32] C. Huang, I. V. Tokatly, and M. A. Cazalilla, Phys. Rev. Lett. **127**, 176801 (2021).

[33] P. Laczkowski, Y. Fu, H. Yang, J.-C. Rojas-Sánchez, P. Noel, V. T. Pham, G. Zahnd, C. Deranlot, S. Collin, C. Bouard, P. Warin, V. Maurel, M. Chshiev, A. Marty, J.-P. Attané, A. Fert, H. Jaffrès, L. Vila, and J.-M. George, Phys. Rev. B **96**, 140405(R) (2017).

[34] M. Yamanouchi, L. Chen, J. Kim, M. Hayashi, H. Sato, S. Fukami, S. Ikeda, F. Matsukura, and H. Ohno, Appl. Phys. Lett. **102**, 212408 (2013).

[35] D. V. Fedorov, C. Herschbach, A. Johansson, S. Ostanin, I. Mertig, M. Gradhand, K. Chadova, D. Ködderitzsch, and H. Ebert, Phys. Rev. B **88**, 085116 (2013).

[36] P. M. Levy, H. Yang, M. Chshiev, and A. Fert, Phys. Rev. B **88**, 214432 (2013).

[37] B. Gu, Z. Xu, M. Mori, T. Ziman, and S. Maekawa, J. Appl. Phys. **117**, 17D503 (2015).

[38] Z. Xu, B. Gu, M. Mori, T. Ziman, and S. Maekawa, Phys. Rev. Lett. **114**, 017202 (2015).

[39] Y. Niimi, M. Morota, D. H. Wei, C. Deranlot, M. Basletic, A. Hamzic, A. Fert, and Y. Otani, Phys. Rev. Lett. **106**, 126601 (2011).

[40] K. Tian and A. Tiwari, Sci. Rep. **9**, 3133 (2019).

[41] R. Ramaswamy, Y. Wang, M. Elyasi, M. Motapothula, T. Venkatesan, X. Qiu, and H. Yang, Phys. Rev. Appl. **8**, 024034 (2017).

[42] S. Lowitzer, M. Gradhand, D. Ködderitzsch, D. V. Fedorov, I. Mertig, and H. Ebert, Phys. Rev. Lett. **106**, 056601 (2011).

[43] M. Obstbaum, M. Decker, A. K. Greitner, M. Haertinger, T. N. G. Meier, M. Kronseder, K. Chadova, S. Wimmer, D. Ködderitzsch, H. Ebert, and C. H. Back, Phys. Rev. Lett. **117**, 167204 (2016).

[44] A. Musha, Y. Kanno, and K. Ando, Phys. Rev. Mater. **3**, 054411 (2019).

[45] T. Ando, Phys. Rev. B **44**, 8017 (1991).

[46] K. Xia, M. Zwierzycki, M. Talanana, P. J. Kelly, and G. E. W. Bauer, Phys. Rev. B **73**, 064420 (2006).

[47] A. A. Starikov, Y. Liu, Z. Yuan, and P. J. Kelly, Phys. Rev. B **97**, 214415 (2018).

[48] A. Lichanot, C. Larrieu, R. Orlando, and R. Dovesi, J. Phys. Chem. Solids **59**, 7 (1998).

[49] K. Hoang and S. D. Mahanti, Phys. Rev. B **78**, 085111 (2008).

[50] F. Tasnádi, M. Odén, and I. A. Abrikosov, Phys. Rev. B **85**, 144112 (2012).

[51] J. Ziman, *Electrons and Phonons* (Oxford University Press, New York, 1960).

[52] Z. L. Wang, Acta Crystallogr., Sect. A **54**, 460 (1998).

[53] C. L. Fu, A. J. Freeman, E. Wimmer, and M. Weinert, Phys. Rev. Lett. **54**, 2261 (1985).

[54] D. Van Dyck, Ultramicroscopy **109**, 677 (2009).

[55] Y.-N. Zhao, S.-X. Qu, and K. Xia, J. Appl. Phys. **110**, 064312 (2011).

[56] Y. Liu, A. A. Starikov, Z. Yuan, and P. J. Kelly, Phys. Rev. B **84**, 014412 (2011).

[57] Y. Liu, Z. Yuan, R. J. H. Wesselink, A. A. Starikov, M. van Schilfgaarde, and P. J. Kelly, Phys. Rev. B **91**, 220405(R) (2015).

[58] S. Wang, Y. Xu, and K. Xia, Phys. Rev. B **77**, 184430 (2008).

[59] L. Wang, R. J. H. Wesselink, Y. Liu, Z. Yuan, K. Xia, and P. J. Kelly, Phys. Rev. Lett. **116**, 196602 (2016).

[60] R. J. H. Wesselink, K. Gupta, Z. Yuan, and P. J. Kelly, Phys. Rev. B **99**, 144409 (2019).

[61] O. K. Andersen, O. Jepsen, and G. Krier, in *Proceedings of the Miniworkshop on Methods of Electronic Structure Calculations and Working Group on Disordered Alloys* (World Scientific, Singapore, 1995), pp. 63–124.

[62] L. Vitos, *Computational Quantum Mechanics for Materials Engineers: The EMTO Method and Applications* (Springer, London, 2007).

[63] L. V. Pourovskii, A. V. Ruban, L. Vitos, H. Ebert, B. Johansson, and I. A. Abrikosov, Phys. Rev. B **71**, 094415 (2005).

[64] Z. Chen, Q. Zhang, Y. Zhang, L. Wang, M. Sang, and Y. Ke, Phys. Rev. B **102**, 035405 (2020).

[65] L. Wang, T. Min, and K. Xia, Phys. Rev. B **103**, 054204 (2021).

[66] L. Wang, T. Min, and K. Xia, Phys. Rev. B **107**, L220402 (2023).

[67] L. Wang, K. Shen, S. S. Tsirkin, T. Min, and K. Xia, Appl. Phys. Lett. **120**, 012403 (2022).

[68] Z. Chen, Q. Zhang, Z. Yuan, J. Liu, K. Xia, and Y. Ke, Phys. Rev. B **107**, 195431 (2023).

[69] A. Hamzć, S. Senoussi, I. Campbell, and A. Fert, Solid State Commun. **26**, 617 (1978).

[70] A. Crépieux, J. Wunderlich, V. Dugaev, and P. Bruno, J. Magn. Magn. Mater. **242-245**, 464 (2002).

[71] S. Takahashi and S. Maekawa, Sci. Technol. Adv. Mater. **9**, 014105 (2008).

[72] G. Y. Guo, J. Appl. Phys. **105**, 07C701 (2009).

[73] T. Tanaka, H. Kontani, M. Naito, T. Naito, D. S. Hirashima, K. Yamada, and J. Inoue, Phys. Rev. B **77**, 165117 (2008).

[74] G. Y. Guo, S. Murakami, T.-W. Chen, and N. Nagaosa, Phys. Rev. Lett. **100**, 096401 (2008).

[75] T. H. Davis and J. A. Rayne, Phys. Rev. B **6**, 2931 (1972).

[76] P. Blood and D. Grieg, J. Phys. F: Met. Phys. **2**, 79 (1972).

[77] J. M. Blakely, Crit. Rev. Solid State Mater. Sci. **7**, 333 (1978).

[78] B. Coester, G. Wong, Z. Xu, J. Tang, W. Gan, and W. Lew, J. Magn. Magn. Mater. **523**, 167545 (2021).

[79] Z. Chi, Y.-C. Lau, X. Xu, T. Ohkubo, K. Hono, and M. Hayashi, Sci. Adv. **6**, eaay2324 (2020).

[80] J.-Y. Kim, D.-S. Han, M. Vafaee, S. Jaiswal, K. Lee, G. Jakob, and M. Kläui, Appl. Phys. Lett. **117**, 142403 (2020).